J Sol-Gel Sci Technol (2017) 81:645–651
DOI 10.1007/s10971-016-4257-z

ORIGINAL PAPER: DEVICES BASED ON SOL-GEL OR HYBRID MATERIALS

Cr-doped TiO_2-based dye-sensitized solar cells with Cr-doped TiO_2 blocking layer

Morteza Asemi[1,2] · **Saeedeh Maleki**[1,2] · **Majid Ghanaatshoar**[1,2]

Received: 14 May 2016 / Accepted: 7 November 2016 / Published online: 15 November 2016

Abstract Cr-doped TiO_2 nanoparticles were synthesized by chemical sol–gel method. The anatase phase of TiO_2 nanoparticles was proved by X-ray diffraction analysis. Furthermore, the field emission scanning electron microscopy revealed that the size of the nanoparticles was about 30 nm. TiO_2 nanoparticles with 0.5 % Cr dopant concentration were selected to fabricate dye-sensitized solar cells due to their smaller band gap. Furthermore, Cr-doped TiO_2 thin films (0.5 %) with different thicknesses were employed as blocking layer on the surface of fluorine-doped tin oxide (FTO) substrate. The current density–voltage measurement showed that the photovoltaic parameters of the fabricated dye-sensitized solar cells were improved after introducing Cr-doped TiO_2 blocking layer at the interface of FTO and Cr-doped TiO_2 mesoporous layer. The maximum power conversion efficiency increased more than 110 % as a result of inserting the Cr-doped blocking layer. The electrochemical impedance spectroscopy indicated that a more efficient charge transfer process takes place at the interface of the FTO/TiO_2 due to the enhanced interfacial properties and reduction of charge recombination.

Graphical Abstract

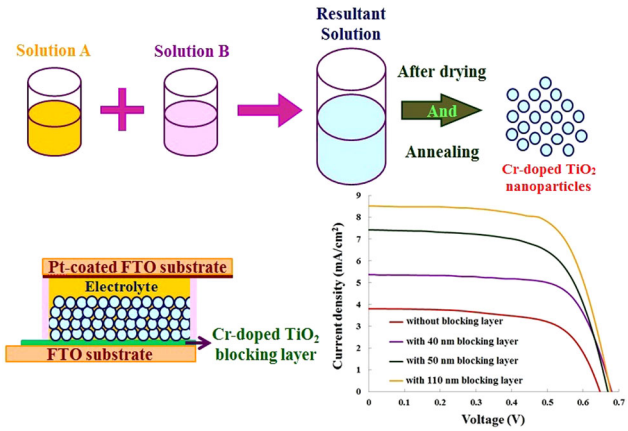

Keywords Dye-sensitized solar cells · Cr-doped TiO_2 · Blocking layer · Sol–gel method

1 Introduction

The photovoltaic technologies have attracted considerable research attention because solar energy is a clean and limitless energy resource compared to the traditional fossil energy sources such as natural gas, coal, and oil [1, 2]. Dye-sensitized solar cells (DSSCs) are considered as one of the promising alternatives to conventional photovoltaic technologies due to the low-cost, easy manufacturing process, lightweight, flexibility, and competitive power conversion efficiency [3–5]. A typical DSSC has very simple structure consisting of a dye-sensitized nanoporous semiconductor photoanode fabricated on fluorine-doped tin oxide (FTO)

✉ Majid Ghanaatshoar
m-ghanaat@sbu.ac.ir

[1] Laser and Plasma Research Institute, Shahid Beheshti University, G.C., Evin 1983969411, Tehran, Iran

[2] Solar Cells Research Group, Shahid Beheshti University, G.C., Evin 1983969411, Tehran, Iran

substrate, a liquid electrolyte containing a redox couple (iodine/iodide) filling the pores of the photoanode and a platinum-coated FTO glass as counter electrode [6–8]. Until now, different types of metal oxide semiconductors have been used in DSSCs (such as TiO_2, ZnO, SnO_2, NiO, $CuCrO_2$) [9–14], but titanium dioxide with anatase phase because of unique photovoltaic and photochemical properties such as high chemical stability, suitable band gap (about 3.2 eV) and ideal position of the conduction band edge has been recognized as the most appropriate metal oxide semiconductor for DSSCs [15, 16]. The position of the TiO_2 conduction band edge lies just below the LUMO level of the N719 dye and facilitates electron injection [17].

To achieve a high efficiency DSSC, a large surface area of the mesoporous TiO_2 layer is essential to load a large amount of dye molecules [10, 18]. Beside this, good connections between the TiO_2 nanoparticles in mesoporous photoanode as well as a good adhesion to the FTO substrate is required to reduce the reaction of photogenerated electrons with the tri-iodide species in electrolyte [19]. Recombination of electrons in FTO conduction band with oxidized dye molecules and the I^{-3} ions present in the I^-/I^{-3} redox couple has a detrimental effect on the conversion efficiency of DSSCs [20–23]. By reducing the electron recombination reaction rate of FTO conduction band electron with oxidized dye molecules and acceptors in the electrolyte, we can improve the efficiency of DSSCs. The ways to minimize interfacial recombination dynamics are employing either titanium tetrachloride ($TiCl_4$) treatment or thin blocking layers of insulating oxides or high-band-gap semiconductors with conduction band edges between those of FTO and TiO_2 mesoporous structure [24–27]. In many studies, $TiCl_4$ treatment was used as a chemical treatment for improving the adhesion of the TiO_2 mesoporous layer to the FTO substrate and blocking charge recombination at the interface [24, 25]. Liu et al. reported the performance improvement of DSSCs with using ZnO blocking layer [28]. Jeong and Kim utilized a thin TiO_2 layer to decrease the recombination of electrons at the FTO/electrolyte interface [29]. Furthermore, Al_2O_3 thin film was employed as charge-recombination barrier in DSSCs by Lin et al. [30].

In recent years, metal-doped TiO_2 nanoparticles were proposed as another way to enhance the efficiency of DSSCs through improving the electron transport in mesoporous TiO_2 layer [31, 32]. The doping technique is one of the promising approaches to improve the electrical conductivity of metal oxide semiconductors. Nikolay et al. have reported an increase in efficiency of DSSCs fabricated from Nb-doped TiO_2 electrode [33]. Sn-, Cu- and Fe-doped TiO_2 have also been studied as the photoanodes in DSSCs and showed power conversion efficiency enhancement [34]. Furthermore, in order to improve the electrochemical properties of the DSSCs such as open-circuit voltage (V_{OC}) and electron transfer rate, recently, influence of Al and Zn co-doping in TiO_2 nanoparticles was studied by Jin et al. [35]. On the other hand, Cr-doped TiO_2 has received much attention because Cr ion can excellently extend the visible light absorption and improve the photocatalytic activity of TiO_2 [36]. The metal dopant incorporated into TiO_2 crystal lattice can form an impurity energy level within the TiO_2 band gap, which allows photons with some lower energy to excite photocatalyst to exhibit visible light activity [37]. The presence of chromium in the structure of TiO_2 can also enhance the conductivity of TiO_2 [38].

In this paper, we investigate the effect of Cr dopant concentration on the structural and optical properties of TiO_2 nanoparticles. The sol–gel method is used for preparation of TiO_2 nanoparticles. Then, we will fabricate DSSCs with Cr-doped TiO_2 nanoparticles. The effect of Cr-doped TiO_2 barrier layer on the efficiency of the DSSCs is also investigated. Regarding the consistency between the physical properties of the Cr-doped layer and those of the photoanode, it is reasonable to expect that the charge transport mechanism is improved. On the other hand, interfacial adhesion between FTO and the mesoporous Cr-doped TiO_2 layer is enhanced by using the Cr-doped TiO_2 compact layer, which increases the short-circuit current density.

2 Experimental details

The Cr-doped TiO_2 nanopowders were prepared by sol–gel method. Titanium tetraisopropoxide (TTIP) solution ($C_{12}H_{28}O_4$.Ti, Aldrich) and chromium nitrate (Cr $(NO_3)_3.9H_2O$, Merck) were used as the titanium and dopant source, respectively. In order to achieve the desired amount of dopant content in Cr-doped TiO_2, initially, the stoichiometric amount of chromium nitrate was dissolved in 10 mL distilled water at room temperature. In other words, the Cr dopant value was adjusted by controlling the amount of Cr $(NO_3)_3.9H_2O$. In order to keep the pH of the prepared solution (solution A) at 2, acetic acid was used. At higher pH values, the crystallinity of the prepared nanoparticles is destroyed and the prepared nanoparticles get amorphous phase. Adding acetic acid also helps in spontaneous nucleation of a large number of very tiny TiO_2 particles during the synthetizing process [39]. Then, 14 mL of TTIP was dissolved in 40 mL of anhydrous ethanol under constant stirring to obtain a homogeneous solution (B). Subsequently, the solution B was added dropwise into the solution A under vigorous stirring at room temperature. The attained sol was stirred for 2 h and aged for 4 days at room temperature. The obtained gels were dried for 10 h at 80 °C. The obtained powders were crushed to fine powders and

finally annealed at 450 °C for 2 h. The undoped TiO_2 was also prepared using the same method for comparative purposes.

Cr-doped TiO_2 thin film was deposited as a blocking layer onto FTO glass by the sol–gel spin-coating technique. Cr-doped TiO_2 sol was prepared by mixing the TTIP, chromium nitrate nonahydrate, and citric acid as precursor materials in ethylene glycol solvent. The molar ratio between precursor materials and solvent was 1:6:0.5:24. The prepared solution was mixed on magnetic stirrer at 90 °C for 30 min until the solution became clear and transparent. The resultant sol was deposited by spin coating onto FTO glass with different speeds (500, 3000, and 6000 rpm) to obtain various thicknesses. The Cr-doped TiO_2 barrier layers were annealed at 500 °C for one hour.

For preparation of DSSCs, the Cr-doped TiO_2 mesoporous layers were deposited onto the Cr-doped TiO_2 barrier layer/FTO/glass substrate using the doctor blade technique. The prepared photoelectrodes were annealed at 450 °C for 30 min with a programmable heating furnace. Cr-doped TiO_2 photoelectrodes were cooled to 80 °C and then immersed in 0.3 mM N719 dye in anhydrous ethanol for 24 h. Then, the samples rinsed with ethanol to remove excess dye and dried at room temperature. The electrolyte was composed of 0.5 M lithium iodide (LiI), 0.05 M iodine (I_2) and 0.05 M tert-butylpyridine dissolved in acetonitrile. A platinized counter electrode was clipped onto the top of the photoanode to create a DSSC. The effective area of the photoelectrodes was 0.25 cm^2.

The crystalline phases of the prepared Cr-doped TiO_2 powders were characterized by powder X-ray diffractometer (XRD) at room temperature using Cu Kα radiation ($\lambda = 0.154056$ nm). The morphology of the synthesized powders was examined by field-emission scanning electron microscope (FESEM, TESCAN mira 3 xmu, Czech). The absorption spectra of the synthesized Cr-doped TiO_2 powders were investigated by 3648 UV–Vis Avantes spectrometer. The thickness of the prepared Cr-doped TiO_2 blocking layers was measured by a profilometer (Dektak XT, Bruker). The photocurrent density–voltage (J–V) characteristics were obtained under illumination of an AM1.5 solar simulator (SIM-1000, Sharif Solar, Iran) using an I-V Tracer (IV-25, Sharif Solar, Iran). In order to investigate the charge transport mechanism at the FTO/electrolyte interface, the electrochemical impedance spectroscopy (EIS) measurement was performed using a potentiostat/galvanostat (IVIUM, Compactstat, Ivium Technologies BV, Netherlands) under AM1.5G simulated solar illumination at 100 $mWcm^{-2}$. EIS spectra were recorded over a frequency range of 100 kHz-0.1 Hz. The applied bias voltage and AC amplitude were fixed at open-circuit voltage (V_{OC}) of the cells and at 10 mV, respectively.

3 Result and discussion

By XRD studies, we determine crystalline structure of the Cr-doped TiO_2 nanoparticles. Figure 1 shows the X-ray diffraction patterns of the Cr-doped TiO_2 nanoparticles annealed at 450 °C. According to the standard XRD patterns of TiO_2, the prepared nanoparticles are single phase anatase structure (JCPDS, No. 21-1272) without any secondary phase or impurity oxide [36, 37]. Therefore, we can conclude that Cr^{3+} (with ionic radius of 0.0755 nm) has been successfully incorporated into the crystal lattice of TiO_2 due to the nearly identical ionic radius to that of the Ti^{4+} cation (0.0745 nm) [37]. In general, as the doping concentration increases, the lattice parameters of the host change according to Vegard's law due to the generation of strain in the crystal lattice of the host material and the diffraction peaks shift toward higher or lower angles with regard to the ionic radius of the dopant [40]. As a result, the presence of the Cr impurity may deteriorate the crystal quality which can be deduced from increase in the full width at half maximum with doping concentration. In order to obtain the average crystallite size of Cr-doped TiO_2 nanoparticles, the Debye–Scherrer equation is used [41]. The crystallite size of the nanoparticles is about 12.1, 10.4, 9.2, and 8.6 nm for undoped and 0.1, 0.5, and 1.0 % Cr-doped TiO_2, respectively. As can be seen, the crystallite size decreases with increasing the Cr dopant concentration. Furthermore, no noticeable peak shift is observed for Cr-doped TiO_2 nanoparticles compared with undoped one, which might be due to the low dopant concentration. These results are in good agreement with those reported by Peng et al. [36].

Figure 2 shows the FE-SEM images of the synthesized undoped and Cr-doped TiO_2 nanoparticles after annealing.

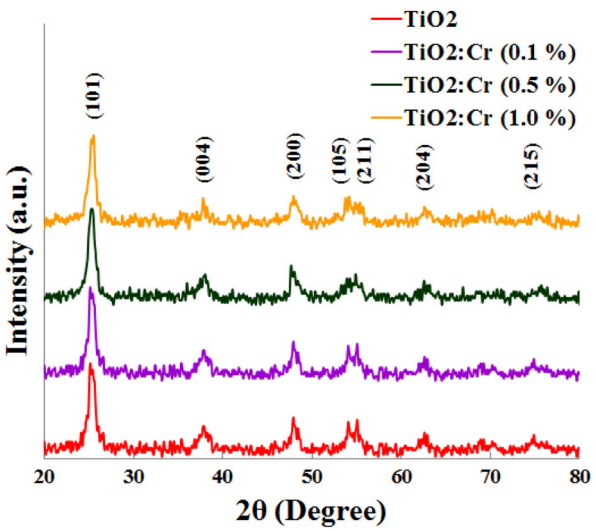

Fig. 1 XRD patterns of the prepared TiO_2 nanoparticles with different Cr-doping concentrations

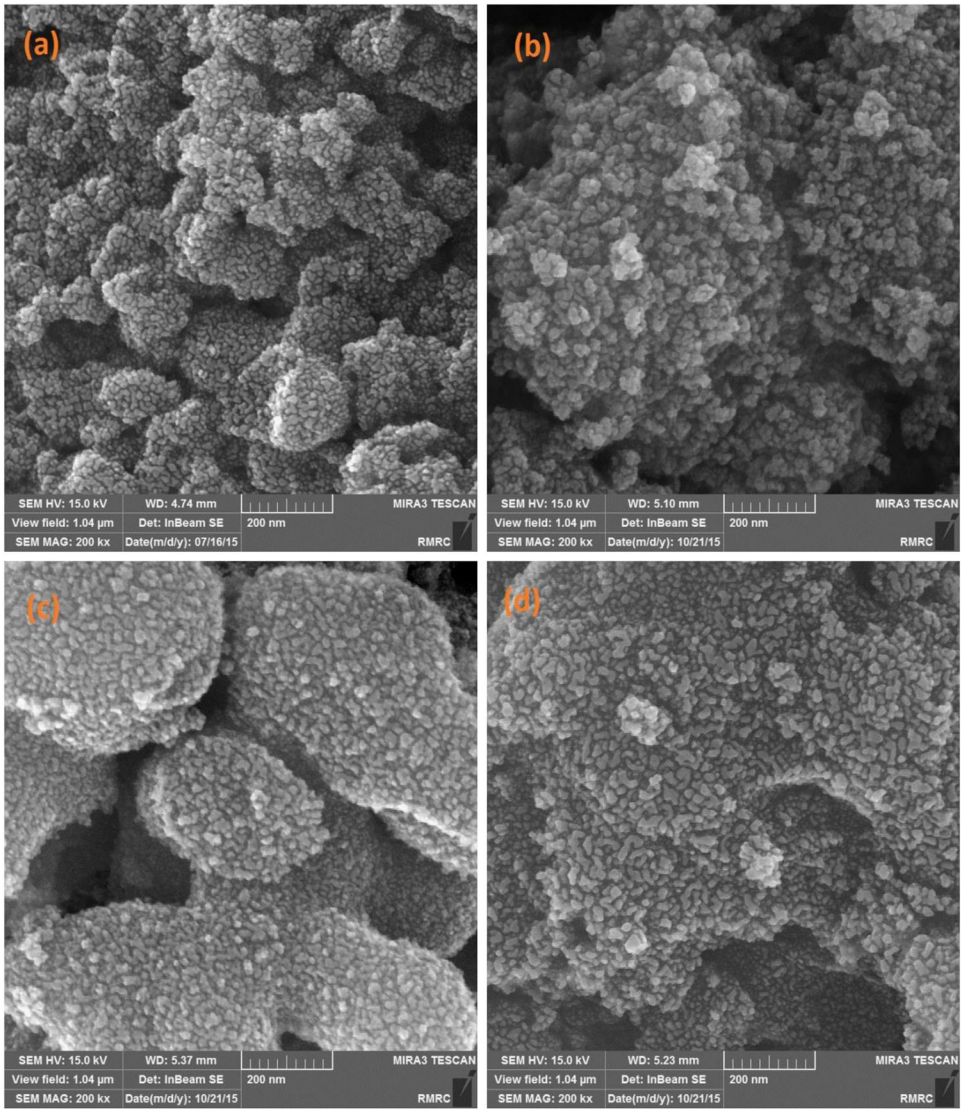

Fig. 2 SEM images of **a** undoped and **b** 0.1 %, **c** 0.5 % and **d** 1.0 % Cr-doped TiO_2 nanoparticles

The morphology of most of the Cr-doped TiO_2 nanoparticles is spherical in shape. In addition, aggregation of the nanoparticles could be obviously observed in FE-SEM images of the samples. The size of the prepared nanoparticles obtained from FE-SEM is around 30 nm. Regarding the results of XRD experiment, it can be inferred that the size of crystallites in the nanoparticles is apparently less than the nanoparticles size which indicates that the produced particles are in polycrystalline phase. It should be noted that a crystallite is defined as the smallest uniform crystallographic unit based on the disorientation to its neighbors. A particle is often consists of more than one crystallite which are in different orientations relative to each other. XRD gives the average crystallite size, not the particle size. However, sometimes we find good agreement between particle size obtained from microscopy images and XRD analysis, especially in the case of nanoparticles [41]. This may be the case where the nanoparticles are single crystalline.

UV–Vis spectroscopy is employed to study the optical properties of the prepared nanoparticles. Aqueous suspensions of the nanoparticles are used for the UV–Vis absorption studies. One milligram of synthesized nanoparticles is dispersed in 100 mL of ethanol by ultrasonic and at least 1 ml of the prepared aqueous sample is used for measurement in a standard quartz cuvette [42]. Figure 3 presents the optical absorption of all Cr-doped and undoped TiO_2 nanoparticles. As can be seen, the absorption edge of undoped TiO_2 nanoparticles appears at around 320 nm, corresponding to the band-gap energy of 3.9 eV. The TiO_2 absorption edge significantly shifts to higher wavelengths with substitution of Cr atoms for Ti atoms. Similarly, light absorption in the visible light region increases with Cr concentration. The optical band gap of the synthesized

nanoparticles is estimated by the Tauc relation. The obtained optical band gaps are 3.9, 3.6, 3.4, and 3.8 eV for undoped, 0.1, 0.5, and 1 % Cr-doped TiO_2 nanoparticles, respectively. The optical band gap initially decreases with Cr concentration and then increases. The decrease in the band gap with Cr dopant concentration can be attributed to (i) the localized states near the valence band of the TiO_2 and (ii) the formation of color centers, which are associated with the oxygen vacancies in TiO_2 or to the radicals in the titanium dioxide lattice associated with the doping ions [43]. The increase in the value of the bandgap for 1 % Cr-doped TiO_2 nanoparticles can be ascribed to hardness of the nanoparticles. According to our experimental observation, the hardness of the prepared nanoparticles increases at higher value of doping concentration (>1 %). Previously, Tse et al. studied the relationship between the hardness of a crystal and its bandgap [44]. They found that the bandgap of a crystal increases alongside hardness. Furthermore, according to Chowdhury et al. report on the relation between the hardness and absorption coefficient, the hardness and absorption coefficient of the materials can be affected by formation of the weak or strength chemical bond between the elements [45]. In comparison with other Cr-doped nanoparticles, the reduction in the absorbance of the 1 % Cr-doped TiO_2 nanoparticles may be due to this effect.

In the next step, TiO_2 nanoparticles with 0.5 % Cr dopant concentration was chosen to fabricate the DSSCs due to their smaller band gap. Furthermore, Cr-doped TiO_2 thin films (0.5 %) with different thicknesses were employed as blocking layer on the surface of FTO substrate. The thickness of the blocking layer was controlled by speed of spin-coating rotation. In this way, we could achieve thin films with thicknesses of 40, 50 and 110 nm. As we expected, after introducing Cr-doped TiO_2 blocking layer at the interface of FTO and TiO_2 mesoporous layer, the photovoltaic parameters were improved. The photocurrent density–voltage (J–V) curves of the solar cells with and without Cr-doped TiO_2 blocking layers are presented in Fig. 4. Moreover, the photovoltaic parameters of all the cells are listed in Table 1. The short-circuit current density (J_{SC}) of the fabricated DSSCs increases with increasing the thickness of the blocking layer. In particular, in the case of fabricated 110 nm-thick Cr-doped TiO_2 thin film, the device gives a great improvement of J_{SC} about 8.52 mA/cm^2. Its power conversion efficiency (η) is 3.92 %, which is 118 % higher than that of the DSSC without a blocking layer. With the use of the blocking layer, the recombination sites are reduced and the charge recombination in the DSSC is effectively suppressed [46]. The blocked FTO/electrolyte interface efficiently prohibits injected electrons into the conduction band of FTO from recombination with the redox couple in electrolyte [47]. Then, the reduced recombination reaction leads to J_{SC} and η enhancement.

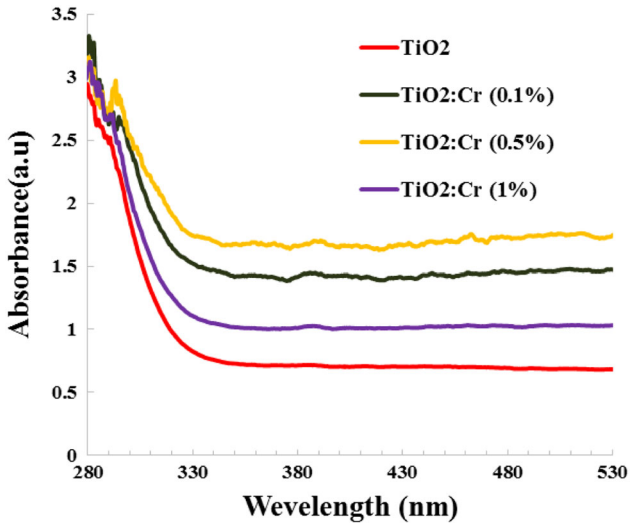

Fig. 3 UV–Vis absorption spectra of the synthesized Cr-doped TiO_2 nanoparticles

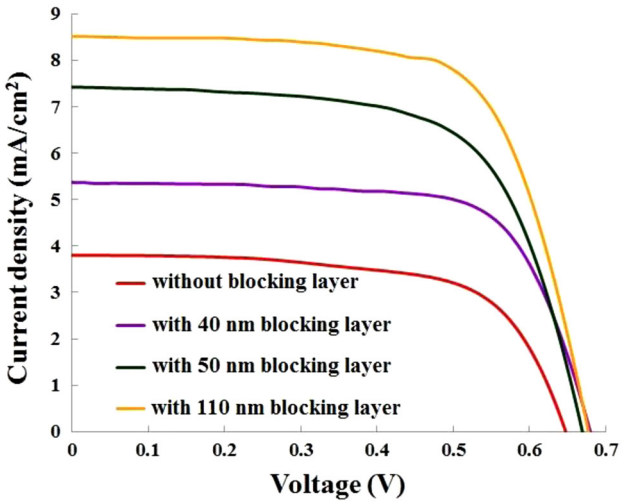

Fig. 4 Current density-voltage curves of the fabricated Cr-doped TiO_2-based DSSCs including Cr-doped TiO_2 thin film as blocking layer

Table 1 Photovoltaic properties of the constructed DSSCs with different thicknesses of blocking layer

Sample	FF (%)	V_{OC} (V)	J_{SC} (mA/cm^2)	η (%)
Without blocking layer	65	0.65	3.79	1.80
With 40 nm blocking layer	70	0.68	5.37	2.56
With 50 nm blocking layer	64	0.67	7.42	3.22
With 110 nm blocking layer	67	0.68	8.52	3.92

DSSCs: dye-sensitized solar cells

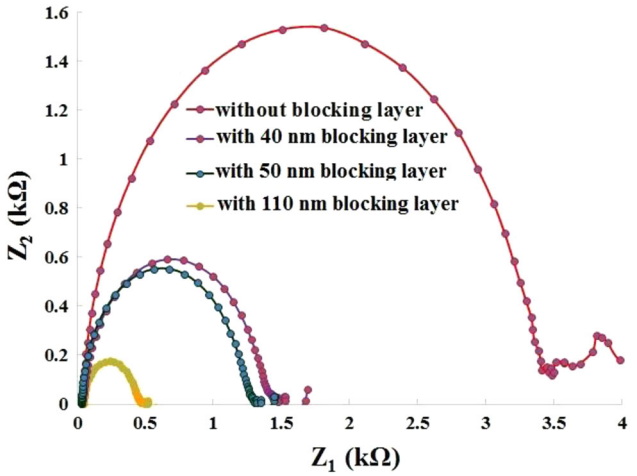

Fig. 5 Nyquist plots of Cr-doped TiO_2-based DSSCs with different thicknesses of Cr-doped TiO_2 thin film as blocking layer

In order to elucidate the electron transport and recombination in the constructed DSSCs, electrochemical impedance spectroscopy (EIS) measurements were carried out as a function of frequency between 0.1 Hz and 100 kHz under one-sun illumination (AM1.5) [48]. An applied bias voltage was set to the open-circuit voltage (V_{OC}) of the DSSCs and AC amplitude of 10 mV was applied. At open-circuit voltage, no current passes through the external circuit and all of the electrons injected into the conduction band react with I^{3-} at TiO_2/electrolyte interface. In the Nyquist plots of EIS spectra, there are two sets of semicircles, each set including a small semicircle at high frequency and a large semicircle at low frequency. As mentioned in the literature [49], the small semicircle at high-frequency region (10^5–10^3 Hz) is attributed to the charge transport at the FTO/TiO_2 and Pt counter electrode/electrolyte interfaces, and the large semicircle in the low-frequency region (10^3–10^0 Hz) is related to the electron transfer at the oxide/dye/electrolyte interface. Figure 5 shows the Nyquist plots of the fabricated DSSCs with different thicknesses of the Cr-doped TiO_2 blocking layer. As can be seen from Fig. 5 the diameter of the second semicircle decreases with increasing the thickness of the blocking layer. This indicates that a more efficient charge transfer process takes place at the interface of the FTO/TiO_2 because of the enhanced interfacial properties and reduction of charge recombination [50].

4 Conclusions

In summary, Cr-doped TiO_2 nanoparticles were synthesized by chemical sol–gel method. We studied the influence of Cr dopant concentration on the structural and optical properties of TiO_2 nanoparticles. The results showed that the prepared nanoparticles had anatase phase and the size of the nanoparticles was about 30 nm. TiO_2 nanoparticles with 0.5 % Cr dopant concentration were chosen to fabricate the DSSCs due to their small band gap. Furthermore, Cr-doped TiO_2 thin films (0.5 %) with different thicknesses were employed as blocking layer on the surface of FTO substrate. The obtained results showed that the photovoltaic parameters of the constructed DSSCs were improved after introducing blocking layer at the interface of FTO and Cr-doped TiO_2 mesoporous layer. The electrochemical impedance spectroscopy revealed that the recombination rate decreases with increasing the thickness of the blocking layers.

Compliance with ethical standards

Conflict of interest The authors declare that they have no competing interests.

References

1. Meng L, Li C (2011) Blocking layer effect on dye-sensitized solar cells assembled with TiO_2 nanorods prepared by dc reactive magnetron sputtering. Nanosci Nanotechnol Lett 3:181–185
2. Giribabu L (2015) Green materials for tapping solar energy. Int J Lumin Appl 5:175–177
3. Moradzaman M, Mohammadi MR (2015) Development of an aqueous TiO_2 paste in terms of morphological manipulation of nanostructured photoanode electrode of dyesensitized solar cells. J Sol-Gel Sci Technol 75:447–459
4. Hocevar M, Berginc M, Topic M, Krasovec UO (2010) Sponge-like TiO_2 layers for dye-sensitized solar cells. J Sol-Gel Sci Technol 53:647–654
5. Jung WH, Kwak NS, Hwang TS, Yi KB (2012) Preparation of highly porous TiO_2 nanofibers for dye-sensitized solar cells (DSSCs) by electro-spinning. Appl Sur Sci 261:343–352
6. Yong SM, Tsvetkov N, Larina L, Ahn BT, Kim DK (2014) Ultrathin SnO_2 layer for efficient carrier collection in dye-sensitized solar cells. Thin Solid Films 556:503–508
7. Cho TY, Yoon SG, Sekhon SS, Kang MG, Han CH (2011) The effect of a sol-gel formed TiO_2 blocking layer on the efficiency of dye-sensitized solar cells. Bull Korean Chem Soc 32:3629–3633
8. Kim JH, Lee KJ, Roh JH, Song SW, Park JH, Yer IH, Moon BM (2012) Ga-doped ZnO transparent electrodes with TiO_2 blocking layer/nanoparticles for dye-sensitized solar cells. Nanoscale Res Lett 11:11–14
9. Mehmood U, Hussein IA, Harrabi K, Mekki MB, Ahmed S, Tabet N (2015) Hybrid TiO_2-multiwall carbon nanotube (MWCNTs) photoanodes for efficient dye sensitized solar cells (DSSCs). Sol Energ Mat Sol Cells 140:174–179
10. Baxter JB, Aydil ES (2006) Dye-sensitized solar cells based on semiconductor morphologies with ZnO nanowires. Sol Energ Mat Sol Celss 90:607–622
11. Lee JH, Park NG, Shin YJ (2011) Nano-grain SnO_2 electrodes for high conversion efficiency SnO_2-DSSC. Sol Energ Mat Sol Cells 95:179–183
12. Rashad MM, Shalan AE (2014) Hydrothermal synthesis of hierarchical WO_3 nanostructures for dye-sensitized solar cells. Appl Phys A 116:781–788
13. Liu Q, Wei L, Yuan S, Ren X, Zhao Y, Wang Z, Zhang M, Shi L, Li D (2015) The effect of $Ni(CH_3COO)_2$ post-treatment on the

charge dynamics in p-type NiO dye-sensitized solar cells. J Mater Sci 50:6668–6676
14. Powar S, Xiong D, Daeneke T, Ma MT, Gupta A, Lee G, Makuta S, Tachibana Y, Chen W, Spiccia L, Cheng YB, Götz G, Bäuerle P, Bach U (2014) Improved photovoltages for p-type dye-sensitized solar cells using $CuCrO_2$ nanoparticles. J Phys Chem C 118:16375–16379
15. Yan J, Zhou F (2011) TiO_2 nanotubes: structure optimization for solar cells. J Mater Chem 21:9406–9418
16. Liu QP (2014) Photovoltaic performance improvement of dye-sensitized solar cells based on Mg-doped TiO_2 thin films. Electrochim Acta 129:459–462
17. Hong Y, Liao JY, Cao D, Zang X, Kuang DB, Wang L, Meier H, Su CY (2011) Organic dye bearing asymmetric double donor-π-acceptor chains for dye-sensitized solar cells. J Org Chem 76:8015–8021
18. Zhi J, Chen A, Cui H, Xie Y, Huang F (2015) NiO-decorated mesoporous TiO_2 flowers for an improved photovoltaic dye sensitized solar cell. Phys Chem Chem Phys 17:5103–5108
19. Zheng H, Neo CY, Mei X, Qiu J, Ouyang J (2012) Reduced graphene oxide films fabricated by gel coating and their application as platinum-free counter electrodes of highly efficient iodide/triiodide dye-sensitized solar cells. J Mater Chem 22:14465–14474
20. Bartelt AF, Schutz R, Strothkamper C, Kastl I, Janzen S, Friedrich D, Fuhrmann WCG, Danner D, Scheller LP, Nelles G, Eichberger R (2014) Solvent-induced surface state passivation reduces recombination in semisquarylium dye-sensitized solar cells. Appl Phys Let 104:223902–223908
21. Nakade S, Kanzaki T, Kubo W, Kitamura T, Wada Y, Yanagida S (2005) Role of electrolytes on charge recombination in dye-sensitized TiO_2 solar cell: the case of solar cells using the I^-/I^{3-} redox couple. J Phys Chem B 109:3480–3487
22. Duong TT, Choi HJ, He QJ, Le AT, Yoon SG (2013) Enhancing the efficiency of dye sensitized solar cells with an SnO_2 blocking layer grown by nanocluster deposition. J Alloys Compd 561: 206–210
23. Patrocínio AOT, Paterno LG, Iha NYM (2009) Layer-by-layer TiO_2 films as efficient blocking layers in dye-sensitized solar cells. J Photochem Photobiol A: Chem 205:23–27
24. Lee SH, Chae SY, Hwang YJ, Koo KK, Joo OS (2013) Influence of TiO_2 nanotube morphology and $TiCl_4$ treatment on the charge transfer in dye-sensitized solar cells. Appl Phys A 112:733–737
25. Lin YH, Wu YC, Lai BY (2012) Collection efficiency enhancement of injected electrons in dye-sensitized solar cells with a Ti interfacial layer and $TiCl_4$ treatment. Int J Electrochem Sci 7:9478–9487
26. Li SJ, Lin Y, Tan WW, Zhang JB, Zhou XW, Chen JM, Chen Z (2010) Preparation and performance of dye-sensitized solar cells based on ZnO-modified TiO_2 electrodes. Int J Miner Metall Mater 17:92–97
27. Gubbala S, Chakrapani V, Kumar V, Sunkara MK (2008) Band-edge engineered hybrid structures for dye-sensitized solar cells based on SnO_2 nanowires. Adv Funct Mater 18:2411–2418
28. Liu Y, Sun X, Tai Q, Hu H, Chen B, Huang N, Sebo B, Zhao XZ (2011) Efficiency enhancement in dye-sensitized solar cells by interfacial modification of conducting glass/mesoporous TiO_2 using a novel ZnO compact blocking film. J Power Source 196:475–481
29. Jeong JA, Kim HK (2011) Thickness effect of RF sputtered TiO_2 passivating layer on the performance of dye-sensitized solar cells. Sol Energ Mat Sol Cells 95:344–348
30. Lin C, Tsai F, Lee MH, Lee CH, Tien TC, Wang LP, Tsai SY (2009) Enhanced performance of dye-sensitized solar cells by an Al_2O_3 charge-recombination barrier formed by low-temperature atomic layer deposition. J Mater Chem 19:2999–3003
31. Manseki K, Ikeya T, Tamura A, Ban T, Sugiuraa T, Yoshida T (2014) Mg-doped TiO_2 nanorods improving open-circuit voltages of ammonium lead halide perovskite solar cells. RSC Adv 4:9652–9655
32. Lu Z, Mou X, Wu J, Zhang D, Zhang L, Huang F, Xu F, Huang S (2010) Improved-performance dye-sensitized solar cells using Nb-doped TiO_2 electrodes: efficient electron injection and transfer. Adv Funct Mater 20:509–515
33. Nikolay T, Larina L, Shevaleevskiy O, Ahn BT (2011) Electronic structure study of lightly Nb-doped TiO_2 electrode for dye-sensitized solar cells. J Energy Environ Sci 4:1480–1486
34. Ako RT, Ekanayake P, Young DJ, Hobley J, Chellappan V, Tan AL, Gorelik S, Subramanian GS, Lim CM (2015) Evaluation of surface energy state distribution and bulk defect concentration in DSSC photoanodes based on Sn, Fe, and Cu doped TiO_2. Appl Sur Sci 351:950–961
35. Jin EM, Jeong SM, Kang HC, Gu HB (2016) Photovoltaic effect of metal-doped TiO_2 nanoparticles for dye-sensitized solar cells. ECS J Solid State Sci Technol 5:109–114
36. Wang C, Shi H, Li Y (2012) Synthesis and characterization of natural zeolite supported Cr-doped TiO_2 photocatalysts. Appl Sur Sci 258:4328–4333
37. Peng YH, Huang GF, Huang WQ (2012) Visible-light absorption and photocatalytic activity of Cr-doped TiO_2 nanocrystal films. Adv Powder Technol 23:8–12
38. Xu H, Zeng M, Li J, Li F (2016) Cr-doped TiO_2 core–shell nanospheres with enhanced photocatalytic activity and lithium storage capacity. Nano 11:1650006
39. Deshpande SB, Potdar HS, Khollam YB, Patil KR, Pasrich R, Jacob NE (2006) Room temperature synthesis of mesoporous aggregates of anatase TiO_2 nanoparticles. Mater Chem Phys 97:207–212
40. Asemi M, Ghanaatshoar M (2016) Controllable growth of vertically aligned Bi-doped TiO_2 nanorod arrays for all-oxide solid-state DSSCs. Appl Phys A 122:853
41. Asemi M, Ghanaatshoar M (2014) Preparation of $CuCrO_2$ nanoparticles with narrow size distribution by sol-gel method. J Sol-Gel Sci Technol 70:416–421
42. Asemi M, Ghanaatshoar M (2016) Conductivity improvement of $CuCrO_2$ nanoparticles by Zn doping and their application in solid-state dye-sensitized solar cells. Ceram Int 42:6664–6672
43. Tian B, Li C, Zhang J (2012) One-step preparation, characterization and visible-light photocatalytic activity of Cr-doped TiO_2 with anatase and rutile bicrystalline phases. Chem Eng Commun 191:402–409
44. Tse JS, Klug DD, Gao F (2006) Hardness of nanocrystalline diamonds. Phys Rev B 73:140102
45. Chowdhury AKMS, Monclus M, Cameron DC, Gilvarry J, Murphy MJ, Barradas NP, Hashmi MSJ (1997) The composition and bonding structure of CN_x films and their influence on the mechanical properties. Thin Solid Films 308:130–134
46. Yu H, Zhang S, Zhao H, Will G, Liu P (2009) An efficient and low-cost TiO_2 compact layer for performance improvement of dye-sensitized solar cells. Electrochim Acta 54:1319–1324
47. Choi H, Nahm G, Kim J, Moon J, Nam S, Jung DR, Park B (2012) The effect of $TiCl_4$-treated TiO_2 compact layer on the performance of dye-sensitized solar cell. Curr Appl Phys 12:737–741
48. Motlak M, Barakat NAM, Akhtar MS, Hamza AM, Yousef A, Fouad H, Yang OB (2015) Influence of GO incorporation in TiO_2 nanofibers on the electrode efficiency in dye-sensitized solar cells. Ceram Int 41:1205–1212
49. Asemi M, Ghanaatshoar M (2016) The influence of magnesium oxide interfacial layer on photovoltaic properties of dye-sensitized solar cells. Appl Phys A 122:842
50. Li W, Yang J, Zhang J, Gao S, Luo Y, Liu M (2014) Improve photovoltaic performance of titanium dioxide nanorods based dye-sensitized solar cells by Ca-doping. Mater Res Bull 57:177–183